

Biomanufacturing of organ-specific tissues with high cellular density and embedded vascular channels

Mark A. Skylar-Scott^{1,2*}, Sébastien G. M. Uzel^{1,2*}, Lucy L. Nam^{1,2}, John H. Ahrens^{1,2}, Ryan L. Truby^{1,2}, Sarita Damaraju^{1,2}, Jennifer A. Lewis^{1,2†}

Engineering organ-specific tissues for therapeutic applications is a grand challenge, requiring the fabrication and maintenance of densely cellular constructs composed of $\sim 10^8$ cells/ml. Organ building blocks (OBBs) composed of patient-specific-induced pluripotent stem cell-derived organoids offer a pathway to achieving tissues with the requisite cellular density, microarchitecture, and function. However, to date, scant attention has been devoted to their assembly into 3D tissue constructs. Here, we report a biomanufacturing method for assembling hundreds of thousands of these OBBs into living matrices with high cellular density into which perfusable vascular channels are introduced via embedded three-dimensional bioprinting. The OBB matrices exhibit the desired self-healing, viscoplastic behavior required for sacrificial writing into functional tissue (SWIFT). As an exemplar, we created a perfusable cardiac tissue that fuses and beats synchronously over a 7-day period. Our SWIFT biomanufacturing method enables the rapid assembly of perfusable patient- and organ-specific tissues at therapeutic scales.

Copyright © 2019
The Authors, some
rights reserved;
exclusive licensee
American Association
for the Advancement
of Science. No claim to
original U.S. Government
Works. Distributed
under a Creative
Commons Attribution
NonCommercial
License 4.0 (CC BY-NC).

INTRODUCTION

The ability to construct whole organs for therapeutic use remains a daunting challenge, requiring billions of cells to be rapidly organized into functional microarchitected units that are supplied with nutrients via pervasive vascular channels (1). Without a readily perfusable circulatory network, engineered human tissues are limited to several hundred micrometers in thickness (2–10). This constraint arises due to the delay between implantation and anastomosis with host vasculature, which necessitates a reliance on the diffusive transport of oxygen and nutrients to maintain cell viability (2, 8, 9). Although avascular tissue grafts may provide a measurable improvement in organ function upon implantation (3, 8, 9), the *de novo* biomanufacturing of three-dimensional (3D) grafts and, ultimately, full-scale organs will inevitably require a perfusable vascular network. While 3D vascularized tissues (~ 1 cm thick) have recently been fabricated via multimaterial 3D bioprinting (11, 12) and stereolithography (13), they lack the requisite cellular density and microstructural complexity needed to achieve physiologically relevant levels of function. Engineered tissues composed of individual cells suspended in extracellular matrices (ECMs), i.e., so-called cells in gels, typically contain at least one to two orders of magnitude lower cell density than those observed *in vivo* (1, 14).

Recent advances in the self-assembly of human embryonic stem cells and induced pluripotent stem cells (iPSCs) have led to the development of organoids that have several characteristics akin in their *in vivo* organ counterparts (15–17). Most organoid protocols [e.g., cerebral (16), kidney (17–19), and cardiac (20) organoids] begin by generating embryoid bodies (EBs) composed of many iPSCs placed into microwells and cultured under static conditions, whose differentiation can be directed into “mini organs” of interest. We posit that these organoids may serve as ideal organ building blocks (OBBs) for biomanufacturing patient- and organ-specific tissues

with the desired cellular density, composition, microarchitecture, and function provided that a perfusible network of vascular channels can be introduced within these living matrices.

Embedded 3D printing offers one viable strategy for achieving this goal. Lewis *et al.* first demonstrated this method by writing a viscoelastic, sacrificial (or fugitive) ink within acellular hydrogel (21) and silicone (22) matrices. After printing, these matrices were cured, and the sacrificial ink was removed, leaving behind a 3D network of interconnected channels. Building on this advance, other researchers developed synthetic (23) and biopolymer (24, 25) matrices that exhibit a self-healing, viscoplastic response that simplifies the patterning of complex 3D architectures. However, to date, these methods have only been used to construct acellular (23, 24) or sparsely cellular (25) matrices.

Here, we report a biomanufacturing method that relies on sacrificial writing into functional tissue (SWIFT) composed of a living OBB matrix to generate organ-specific tissues with high cell density, maturation, and desired functionality (Fig. 1). First, we create hundreds of thousands of iPSC-derived OBBs in the form of EBs, organoids, or multicellular spheroids. Next, these OBBs are placed into a mold and compacted via centrifugation to form a living OBB matrix. We then rapidly pattern a sacrificial ink within this matrix via embedded 3D printing, which upon removal yields perfusable channels in the form of single or branching conduits. Last, we demonstrate that these bulk vascularized tissues function and mature when perfused over long durations.

RESULTS

We grow iPSCs in adherent culture and transfer them into large-scale microwell arrays to form a large volume (> 1 ml) of EBs for SWIFT. After harvesting, these EBs can either be used directly as OBBs (Fig. 1A) or further differentiated into specific organoids of interest. For each SWIFT construct, we cultured and harvested up to 400,000 OBBs, which are subsequently mixed with a tailored ECM solution composed of collagen I and Matrigel held at 0° to 4°C. This ECM solution is ideally suited for creating perfusable vascular channels because its fluid-like behavior at low temperatures facilitates casting

¹Wyss Institute for Biologically Inspired Engineering, Harvard University, Cambridge, MA 02138, USA. ²John A. Paulson School of Engineering and Applied Sciences, Harvard University, Cambridge, MA 02138, USA.

*These authors contributed equally to this work.

†Corresponding author. Email: jalewis@seas.harvard.edu

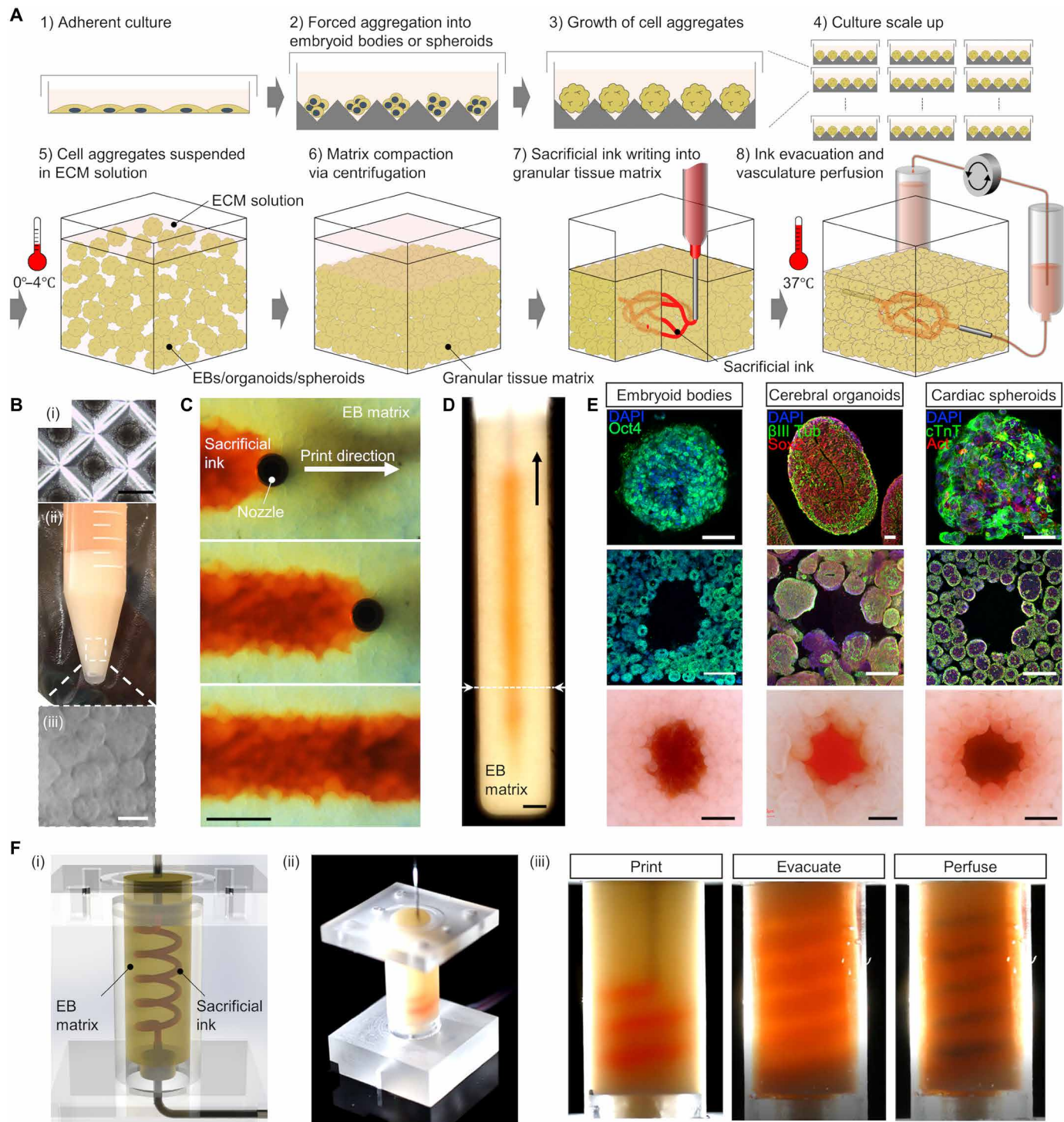


Fig. 1. Sacrificial writing into functional tissue (SWIFT). (A) Step-by-step illustration of the SWIFT process. (B) (i) Large-scale microwell culture of approximately (ii) 2.5 ml of EB-based OBBs, compacted to form an (iii) OBB tissue matrix composed of approximately half a billion cells. Scale bar, 300 μ m (i). Scale bar, is 200 μ m (iii). (C) Time-lapse of sacrificial ink (red) writing via embedded 3D printing within an EB matrix observed from beneath the reservoir. Scale bars, 1 mm (C and D). (D) Front view of a vertical line of sacrificial ink printed within an EB matrix. Scale bars, 1 mm (C and D). (E) Examples of the SWIFT process for different OBB-based matrices composed of the following: (i) EBs, (ii) cerebral organoids, and (iii) cardiac spheroids. Row 1: Individual OBBs with characteristic markers. Rows 2 and 3: Cross sections [as indicated in (D) by the dashed line] of immunostained slices and bright-field images, respectively, of the OBB types. Scale bars, 50 μ m (top row) and 500 μ m (middle and bottom rows). (F) Generation of a helical (vascular) feature in an EB matrix via SWIFT: (i) CAD representation of the system and (ii) corresponding image of sacrificial ink writing within an EB matrix, and (iii) image sequence acquired during embedded 3D printing of a sacrificial ink (left), sacrificial ink evacuation upon incubation (middle), and tissue perfusion using media (dyed blue) through the printed helical vascular channels.

and embedded printing. However, once the SWIFT construct is placed in an incubator at 37°C, the ECM solution undergoes gelation and stiffens markedly to facilitate sacrificial ink removal and subsequent tissue perfusion (3, 4). The cold OBB-ECM slurry is compacted via centrifugation to produce a living tissue matrix (~2.5 ml in volume) that contains nearly half a billion cells at a cell density of ~200 million cells/ml (Fig. 1B). The cold, compacted OBB-ECM slurry provides sufficient support for embedded 3D printing of a sacrificial gelatin ink, which serves as a template for the vascular channel(s) of interest. During SWIFT, we directly observed yielding of tissue matrix roughly 1 mm ahead of the translating cylindrical nozzle and self-healing in its wake (Fig. 1C, fig. S1, and movie S1). Because of its self-healing behavior, the translating nozzle does not generate defects, such as crevasses, within the living tissue matrix. After SWIFT, the tissue construct is warmed to 37°C. The sacrificial gelatin ink melts and is removed, leaving behind a network of tubular channels embedded within the tissue construct. The resulting tissue is immediately connected to an external pump and perfused in oxygenated media to maintain cell viability.

SWIFT can be used to embed vascular channels into living matrices composed of a broad range of OBBs. For example, we printed patent vascular channels into three distinct OBB matrices: compacted EBs, cerebral organoids (after 21 days of differentiation), and beating cardiac spheroids that contain iPSC-derived cardiomyocytes mixed with primary cardiac fibroblasts (Fig. 1, D and E). SWIFT does not adversely affect their complex microarchitecture, as evidenced by the presence of intact ventricle-like structures within individual cerebral organoids in these matrices (fig. S2, A and B). Once warmed, the printed tissue is supported by the surrounding ECM (fig. S2C). Given its free-form nature, one can use SWIFT to pattern nearly arbitrary vascular networks, as highlighted by the 3D helical structure printed and perfused within an EB-based matrix (Fig. 1F and movie S2).

The SWIFT biomanufacturing method requires that the OBB-based matrices initially display the requisite self-healing, viscoplastic response to enable sacrificial ink writing followed by a subsequent stiffening of the matrix to facilitate ink removal (Fig. 2) (26). A crucial component of our OBB matrix design is the engineered ECM, whose stiffness is highly temperature dependent. Following the protocol described above, a cold OBB-ECM slurry is created composed of a nearly monodisperse population of EBs (mean diameter of 212 μ m and a coefficient of variation of 4.7%) (Fig. 2A). Upon compaction, the resulting tissue matrix exhibited a strong shear thinning behavior with a shear yield stress of τ_y ~10 Pa (Fig. 2B and fig. S3). When maintained at 2°C, the tissue matrix exhibits a solid-like response, i.e., its plateau storage modulus (G' , ~200 Pa) exceeds its loss modulus (G'' , ~50 Pa). The sacrificial gelatin ink is designed, such that its shear yield stress (τ_y , ~400 Pa) is at least an order of magnitude higher than that of the matrix (Fig. 2B) (22, 26) to enable the desired cylindrical filaments to be patterned in an omnidirectional manner. During printing, the fluid-like ECM within the tissue matrix contributes minimally to its rheological behavior (fig. S3, B and C). In the absence of densely packed OBBs within the matrix, the cold ECM solution (held at 2°C) exhibited a purely viscous response (η , ~1 Pa) that is not suitable for embedded 3D printing (21). However, upon printing and warming the tissue matrix to 37°C, its plateau shear elastic modulus (G') increases by roughly three orders of magnitude to a value of 280 kPa (Fig. 2C and fig. S3D), as the ECM undergoes thermal gelation to produce a fibrillar gel that occupies the interstitial space between densely packed OBBs. As stated previ-

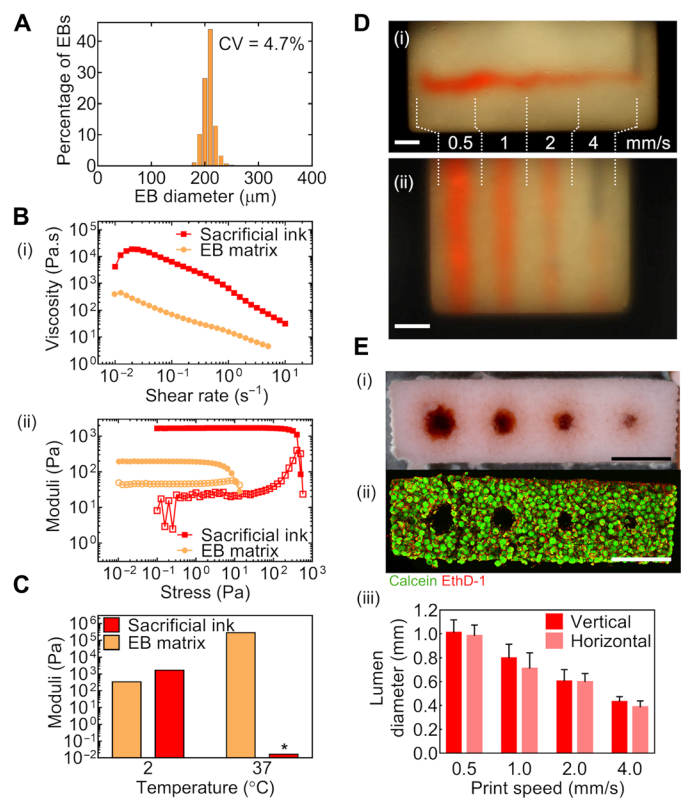


Fig. 2. Living matrix and ink rheology for SWIFT. (A) Size distribution ($n = 413$ EBs) of EBs used to form EB matrices. (B) (i) Apparent viscosity as a function of shear rate and (ii) shear storage (closed markers) and loss moduli (open markers) as a function of shear stress of the EB matrix and sacrificial gelatin ink. (C) Temperature effects on the plateau storage moduli (or loss modulus indicated by an asterisk) of the EB matrix and the sacrificial gelatin ink. (D) SWIFT printing of (i) horizontal and (ii) vertical features (vascular templates) embedded at print speeds of 0.5, 1, 2, and 4 mm/s. (E) Effect of print speed on the lumen diameter shown as (i) bright-field and (ii) viability staining images in the context of vertically printed channels and (iii) lumen (channel) diameter as a function of print speed for vascular templates embedded via horizontal and vertical SWIFT printing. Error bars indicate SD ($n = 4$). Scale bars, 2 mm (D and E). EthD-1, ethidium homodimer-1.

ously, the pronounced increase in tissue matrix stiffness allows it to retain its structural integrity during removal of the sacrificial ink and support pressure-driven flow during subsequent perfusion. As controls, we measured the rheological properties of compacted EBs alone (no ECM) and found that its stiffness substantially increased upon heating from 2° to 37°C. By contrast, the pure ECM rapidly stiffened by roughly two orders of magnitude to a value of 110 Pa under those same conditions (fig. S3E). Hence, by tailoring the tissue matrix composition and sacrificial ink rheology, we developed a system that allows vascular channels to be printed in any arbitrary direction via SWIFT (Fig. 2D). To demonstrate this, we patterned embedded channels with smoothly varying diameters between 400 μ m and 1 mm using a 250- μ m nozzle, through which the sacrificial ink is deposited at a constant volumetric flow rate and varying print speed (Fig. 2E). While there is no upper limit on channel diameter, those below 400 μ m could not be printed with high fidelity since their size approaches the characteristic diameter (d) of the OBBs, in this case ~200 μ m. While smaller EBs would enable higher-feature resolution during SWIFT, the volume of the EB matrix generated decreases as d^3 for a fixed number of microwell arrays. For the print speeds

evaluated (0.5 to 4 mm/s), the shear stress imparted by the nozzle does not adversely affect either the cell viability or matrix integrity, as shown in Fig. 2Eii and fig. S4. The embedded channel features can also be seamlessly connected to form branching vascular networks (fig. S5). We note that the viscoplastic nature of the tissue matrix also allows dense OBB-based inks to be directly printed within it akin to the sacrificial ink. As a simple example, we printed an ink composed of compacted fluorescent protein-expressing EBs into a tissue matrix composed of wild-type (nonfluorescent) EBs in the form of a helical pattern (fig. S6).

To determine cell viability, we manufactured a perfusable EB-based tissue in a perfusion chamber that enables circulation of oxygenated media through the embedded vascular channels and around the periphery of the tissue (Fig. 3A and fig. S7). As a control, we cast a nonperfusable EB-based tissue (referred to as “no channel”) and only flowed media around its periphery in the same chamber (Fig. 3A, top). We find that the control tissue (cross section, 4.2 mm by 4.2 mm) developed a necrotic core within 12 hours with viable, metabolically active cells (per calcein-acetoxymethyl (AM) ester staining) restricted to a narrow “band” (~0.8 mm thick) at the tissue periphery (Fig. 3B and fig. S8). By contrast, luminal perfusion of the perfusable EB-based tissue enhanced cell viability throughout the bulk tissue (Fig. 3B). Their high cell density made it difficult to image the core of individual EBs within these matrices (see fig. S4). Hence, we reported a tissue viability based on the ratio of a thresholded calcein signal (viable cells) to a thresholded nuclear signal (total cells) normalized by the value derived for the full cross section of an avascular tissue composed of the same EBs (Fig. 3Biv). Notably, similar cell viability values are observed initially ($t = 0$ hours) between the perfused and nonperfused (control) tissues (fig. S8) even for EBs located adjacent to the printed lumen, indicating that the SWIFT process has no adverse effects (fig. S4). We also find that tissues subjected to perfusion of normoxic (21% O₂, 5% CO₂) or hyperoxic (95% O₂, 5% CO₂) media (Fig. 3Biv) exhibited similar cell viability values.

To scale up the SWIFT biomanufacturing process, we created a custom-shaped mold (4 mm thick) with a single inlet and outlet for perfusion (fig. S9) and filled it with 2.5 ml of our compacted EB-ECM slurry composed of ~400,000 EBs and a total of 0.5 billion cells. We then printed a branched, hierarchical channel network that is designed to both distribute flow and maintain a constant wall shear stress throughout the tissue matrix (Fig. 3C and movie S3). After printing, the tissue construct is warmed, the sacrificial ink is removed, and the resulting channels are perfused with hyperoxygenated medium (95% O₂, 5% CO₂) at a flow rate of 250 μ l/min. After 12 hours of constant perfusion, the embedded vascular channels remained patent, and the tissue contracts slightly (Fig. 3D, top) as adjacent OBBs fuse together and undergo remodeling. Similar to the smaller tissues (0.2 ml in volume) shown in Fig. 3Bii and iii, cells within these bulk perfusable tissues (2.5 ml in volume) remain viable throughout most of their 4-mm thickness, as indicated by the fluorescence of calcein-AM (Fig. 3D, bottom).

We introduced human umbilical vein endothelial cells (HUVECs) to form endothelial-lined channels within these SWIFT constructs. Specifically, the endothelial cells are seeded by first perfusing a suspension of HUVECs (10⁷ cells/ml) through an embedded, bifurcating vascular network (Fig. 3, E to H, and movie S4) within a SWIFT construct. The cells were allowed to adhere to the luminal surface. Following 20 hours of perfusion, we sliced the opaque tissue longitudinally and directly imaged the endothelialized lumen. While

endothelial cells do form a characteristic cobblestone pattern on some portions of the luminal surface, as indicated by vascular endothelial cadherin (VECad) staining (Fig. 3, G and H), their coverage was incomplete. Our ongoing efforts are focused on producing confluent endothelium within these printed vascular channels.

To further demonstrate SWIFT, we created a functional, perfusable tissue containing human iPSC-derived cardiac OBBs (Fig. 4). Because of its scalability, we adapted a growth factor-free suspension culture protocol that starts from EBs and modulates the Wnt pathway via addition of small molecules to the cell culture medium (27), a strategy that yields cardiomyocytes with a high efficiency (Fig. 4, A to D) (28). Using this protocol, we generated up to 6 ml (upon compaction) of beating cardiac OBBs (movie S5), containing 79 ± 6% cardiomyocytes (cardiac troponin T-positive, cTnT⁺) and 19 ± 6% stromal cells (cTnT⁻, Vimentin⁺) (Fig. 4D and fig. S10). These OBBs were mixed with our engineered ECM and human neonatal dermal fibroblasts (HNDFs) to form a slurry that was subsequently compacted via centrifugation yielding a cardiac tissue matrix (fig. S11). Once compacted, the cardiac matrix had an estimated cell density of 240 million cells/ml and a cardiomyocyte density of 180 million cells/ml (Fig. 4E). When formed into a small disc-shaped mold, this cardiac OBB construct initially beats asynchronously, with calcium waves propagating sporadically and chaotically after a single day (day 1) of perfusion (fig. S12 and movie S6). However, after 7 days in culture (day 7), the tissue construct beats spontaneously and synchronously with calcium waves propagating rhythmically and rapidly throughout the tissue (fig. S12 and movie S6).

Next, we embedded, evacuated, and perfused a branching channel architecture within this cardiac OBB matrix (Fig. 4F and movie S7). To generate multiple samples for analysis, we produced simple tissue constructs that each contain a single printed channel, which is perfused by a luminal flow of 500 μ l/min, resulting in a moderate shear stress of ~0.8 dyn/cm². Each T-shaped tissue is connected to an inlet tube at the bottom and was mounted at the top via a pair of anchoring prongs that serve to both stabilize the tissue and allow one to monitor its contraction and beating over time (fig. S13, A and B). After 1 day of perfusion, the bulk tissue remained viable (Fig. 4G). Over an 8-day period, the cardiac tissue developed a pervasive sarcomeric architecture (Fig. 4H and fig. S13, C and D). Over this same period, the overall tissue contractility increased by more than 20 times, as visualized by the amplitude of anchoring prong motion (Fig. 4I, fig. S13B, and movie S8). A ~40% enhancement in beating capability is obtained upon adding 2 mM calcium to the medium. Beating synchronization also increased, as suggested by coordinated contraction patterns on opposite sides of the tissue section at day 8 (fig. S14). In addition to spontaneous contraction, the tissue responded to paced stimulation via a pair of platinum electrodes situated on either side of the tissue (Fig. 4J and movie S8).

To further characterize the functional performance of cardiac tissue constructs produced by SWIFT biomanufacturing, we perfused isoproterenol, a nonselective agonist for the β -adrenoreceptor, through an embedded channel at a concentration of 10⁻⁵ M, which resulted in a doubling of the spontaneous beating frequency (Fig. 4, K and L). We also perfused 1-heptanol, a gap junction blocker, at a concentration of 1 mM and observed a reduction in their contractile amplitude (Fig. 4, M and N). As a final demonstration, we printed an arterial vascular network geometry within a cardiac OBB matrix using patient-specific, cardiac structural data available from the National Institutes of Health (NIH) 3D Print Exchange (Fig. 4, O and P). We

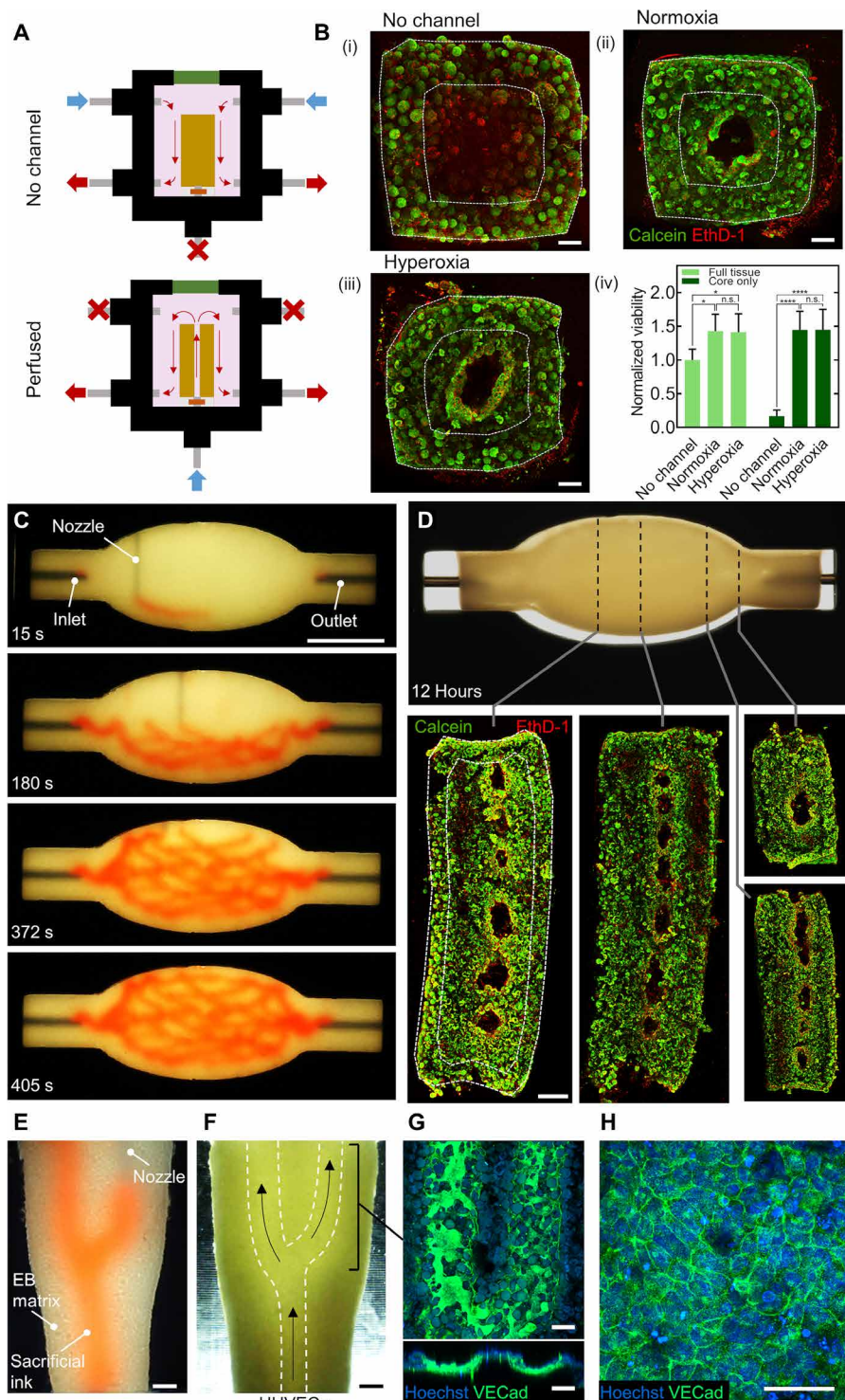


Fig. 3. Perfusionable EB tissue fabricated by SWIFT. (A) Perfusion system used to assess tissue viability following SWIFT printing. (B) Viability staining and analysis following 12 hours of culture of a tissue featuring (i) no channel or perfused with either (ii) normoxic (21% O₂) or (iii) with hyperoxigenated (95% O₂) media along with the corresponding quantification of the (iv) normalized viability. Scale bars, 500 μ m. Error bars indicate SD ($n=4$). The dashed lines highlight viability regions that arise from external perfusion. The “core-only” region corresponds to the area located within the innermost line. (C) An image sequence showing the embedded 3D printing of a branched, hierarchical vascular network within a compacted EB-based tissue matrix connected to inlet and outlet tubes, seen entering the tissue from the left and right. Scale bar, 10 mm. (D) Image of the perfusable tissue construct after 12 hours of perfusion (top) and fluorescence image of LIVE/DEAD (green/red) cell viability stains at various sections through the tissue (bottom). The dashed line represents the equivalent viability depth for an avascular control perfused only from the outside, see (Bi). Scale bars, 1 mm (E and F). (E) SWIFT printing of a bifurcating channel for lumen endothelialization. (F) Evacuated channel (highlighted by the white dashed lines) undergoing the perfusion of HUVEC cells. Scale bar, 1 mm. (G and H) Formation of a VECad-positive monolayer of an HUVEC endothelium. Scale bars, 500 μ m (G) and 50 μ m (H).

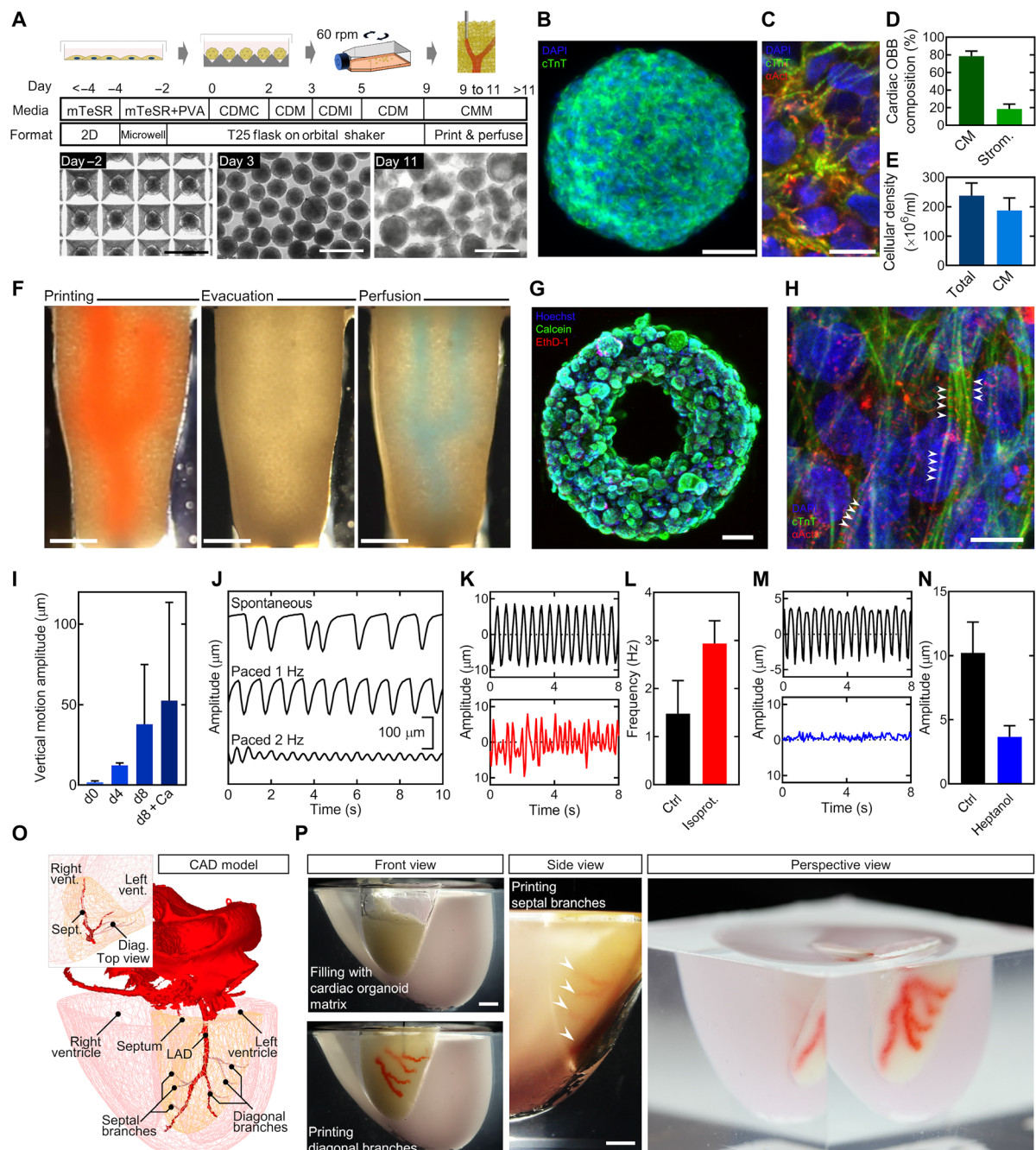


Fig. 4. Perfusionable cardiac tissue fabricated by SWIFT. (A) Cardiac organoid differentiation protocol. (B) Cardiac troponin T and 4',6-diamidino-2-phenylindole (DAPI) staining in a single cardiac OBB at day 9. Scale bar, 50 μ m. (C) Cardiac troponin T, α -actinin, and DAPI staining in a single cardiac OBB at day 9. Scale bar, 10 μ m. (D) Cardiac spheroid composition in iPSC-derived cardiac OBB. Cardiomyocytes (CM) are identified as cardiac troponin T-positive (cTnT $^{+}$) and stromal-like cells (strom.) as cTnT $^{+}$ /Vimentin $^{+}$. (E) Cellular density in compacted cardiac OBB tissue. (F) An image sequence showing the embedding, evacuation, and perfusion of branched vascular channels within a cardiac tissue matrix (tissue dimensions: top width, 6 mm; bottom width, 4.2 mm; depth, 4.2 mm; and height, 12 mm). Scale bars, 2 mm. (G) Viability staining of a SWIFT cardiac tissue (cross section) after 24 hours of perfusion. Scale bar, 500 μ m. (H) cTnT, α -actinin, and DAPI staining in a SWIFT cardiac tissue after 8 days of perfusion that shows evidence of sarcomeric remodeling (arrowheads). Scale bar, 10 μ m. (I) Vertical displacement of the anchoring flexible prongs due to spontaneous cardiomyocyte contraction showing increasing amplitude over time. On day 8, 2 mM calcium is added to the medium to increase cardiomyocyte contractility ("d8 + Ca"). (J) Comparison of anchor displacement pattern between spontaneous contraction and electrical pacing (1 and 2 Hz) of SWIFT cardiac tissues. (K) Spontaneous contraction pattern before and after administration of 10 μ M isoproterenol. (L) Average contraction frequency under isoproterenol treatment. (M) Spontaneous contraction pattern before and after administration of 1 mM 1-heptanol. (N) Maximum peak-to-peak contraction amplitude under 1-heptanol treatment. (O) 3D CAD model of a normal human heart, including a segment of the left anterior descending (LAD) artery and a diagonal branch, downloaded from the National Institutes of Health 3D Print Exchange (additional septal and diagonal branches were added manually, pink). (P) A 1:2 scale polydimethylsiloxane mold is formed using the 3D computed tomography data, and the LAD artery together with diagonal and septal (arrowheads) branches are embedded into a septal-anterior wall wedge [yellow section in (O)] of the cardiac tissue matrix via SWIFT. Scale bar, 5 mm.

used a 3D printed mold to replicate a wedge of the myocardium at a 1:2 scale and, upon filling the mold with a compacted cardiac OBB matrix, used SWIFT to replicate the geometry of the left anterior descending (LAD) coronary artery, which passes anteriorly and then septally and lies adjacent to the outer edge of the cardiac tissue.

DISCUSSION

The SWIFT biomanufacturing method uses densely cellular matrices composed of iPSC-derived OBBs to produce autologous tissues composed of patient-specific cells. This method enables one to create perfusable organ-specific tissues of arbitrary volume and shape in a scalable manner. We estimate that large volumes (100 ml) of perfusable OBB-based tissues could be patterned with an embedded vascular channel network. However, successful translation of these organ-specific tissues for therapeutic applications will require additional advances. For example, current protocols for iPSC-derived organoids yield OBBs that lack sufficient cell maturation and microvascular network formation. Hence, only a modest contractility (~1% strain) is observed for SWIFT cardiac tissues compared to the contractility (~20% strain) observed for adult cardiac tissue (29). We are currently focused on generating anisotropic cardiac OBBs with the aim of further enhancing tissue function, including contractility. In addition, we envision adopting new protocols, such as those recently reported for renal organoids (19), that offer a pathway to creating more mature, microvascularized OBBs. Alternatively, one could enhance tissue function by using living matrices composed of primary cell spheroids harvested from adult tissues for SWIFT. The field of organ engineering is rapidly evolving. For example, other researchers recently reported the embedded 3D printing of a large heart-shaped construct using the traditional “cells in gel” approach. Although this work received considerable attention, those tissues were not perfused long term *in vitro*, and their cell viability and contractile function were not reported (30).

In summary, we have demonstrated a new biomanufacturing method, known as SWIFT, that uses iPSC-derived OBB tissue matrices that exhibit the requisite cell density, microarchitecture, and function approaching that of native tissues. SWIFT can be implemented with a wide range of OBBs, including EBs, differentiated organoids, and multicellular spheroids. Our method opens new avenues for creating personalized organ-specific tissues with embedded vascular channels for therapeutic applications.

MATERIALS AND METHODS

iPSC culture

Personal Genome Project 1 (PGP1) iPSCs or, for all EB-derived cardiac OBB protocols, BJFF iPSCs (provided by S. Jain at Washington University) were cultured on Matrigel-coated plates (Corning Life Sciences) and maintained in mTeSR1 medium (STEMCELL Technologies). Once colonies began to merge (60 to 80% confluence), cells were rinsed with phosphate-buffered saline (PBS) without calcium or magnesium and passaged by adding an enzyme-free passaging solution (ReLeSR, STEMCELL Technologies) at 1 ml/10 cm² of tissue culture area. The ReLeSR was immediately aspirated away, and the flask was incubated for 7 min at 37°C, 5% CO₂. To lift off colonies, fresh mTeSR1 (1 ml/10 cm²) was gently added to the flask using a serological pipette and slowly pipetted back up once to break up the colonies. The cells were then added to a freshly prepared

Matrigel-coated flask, performing a split between 1:8 and 1:3, and mTeSR1 was added to a total volume of 2 ml/10 cm² of tissue culture area. Cells were maintained at 37°C/5% CO₂ in an incubator.

Microwell array fabrication

Microwell array plates were used to generate large numbers (>10⁵) of uniform EBs via forced aggregation. The microwells, in the form of inverted pyramids with 400-μm base width, were arranged in a six-well plate format and manufactured via polydimethylsiloxane (PDMS) molding. The following process was used to facilitate demolding and ensure casting compatibility between polymers. Briefly, SYLGARD 184 (Dow Corning) was mixed 10:1 with its cross-linker and poured into a commercially available microwell plate, degassed in a vacuum chamber, and cured at 80°C for 2 hours to generate a negative cast of the microwells. Next, Ecoflex 00-30 (Smooth-On Inc.) was used to create a positive mold by following a similar method of pouring, degassing, and curing as for the SYLGARD 184. After removing the cured Ecoflex, a two-part polyurethane (Smooth-On Inc.) was poured onto the Ecoflex positive to create a polyurethane-negative mold. Next, ~80 g of SYLGARD 184 was mixed with 8 g of its cross-linker in a planetary mixer, poured into a polyurethane negative mold, degassed for 10 min in a vacuum, and allowed to cure at room temperature for 24 to 48 hours. The cured SYLGARD 184 was then placed in the oven at 80°C for >2 hours to ensure complete cross-linking before removal from the polyurethane mold.

EB formation

To prepare the microwell arrays for cell culture, the arrays were immersed in isopropyl alcohol for 1 hour and then immersed in water and autoclaved for 1 hour. Immediately before preparing the cells, the autoclaved water was drained from the wells, and then, they were placed into a sterile one-well tray (Omnitray, Falcon). Next, 1.5 ml of AggreWell Rinsing Solution (ARS; STEMCELL Technologies) was added per well before centrifuging the wells at 2000g for 5 min to remove trapped air bubbles from the wells. The ARS was aspirated, and the wells were rinsed twice with 2 ml of Dulbecco’s modified Eagle’s medium (DMEM). Last, the DMEM was replaced with 3 ml of EB culture medium (EBCM) supplemented with 10 μM ROCK inhibitor (ROCKi; Y27635; EMD Millipore), and the microwell arrays were maintained at room temperature. To prepare EBCM, mTeSR1 was mixed 1:50 with a polyvinyl alcohol (PVA) stock solution to generate a solution of 4 mg/ml. Penicillin-streptomycin was added to 100 U/ml, and the solution was sterile-filtered and stored at 4°C for up to 2 weeks. The PVA stock solution was prepared by adding 20 g of PVA (30 to 70 kDa; Sigma-Aldrich) to 80 ml of deionized water while stirring at room temperature. Under continuous stirring, the solution temperature was increased to 80°C to fully dissolve PVA in water, after which the PVA solution was stored at 4°C until ready for use.

To form EBs, PGP1 iPSCs were grown to 60 to 80% confluence in Matrigel-coated 225-cm² T225 flasks (Falcon). One T225 of PGP1 cells was typically used to seed 24 wells (four six-well plates), each containing ~4200 microwells. To lift off the iPSCs from the substrate, the cells were first rinsed in PBS without calcium or magnesium and incubated in Accutase (Innovative Cell Technologies) for 15 min at 37°C to generate a mostly single-cell suspension. The cells were added to prewarmed DMEM/F12 and Hepes and centrifuged at 220g for 5 min. The supernatant was removed, and the cells were resuspended in EBCM and 10 μM ROCKi. Cells were counted using

a LIVE/DEAD imaging system, and 1 ml of the cell suspension is seeded into each well at a cell density of approximately 500 cells per microwell. The well plates were then centrifuged at 100g for 3 min to compact the cells. After 24 hours, the cell media was replaced with 4 ml of fresh EBCM to remove the ROCKi. The well plates then underwent two half-media changes (2 ml of EBCM is replaced with fresh media) per day. Care was taken during media changes with media added and removed slowly as to not disturb the EBs from their individual microwells. After 4 days of culture, a total of eight six-well microwell array plates could generate a sufficient volume of EBs to render ~1 ml of OBB slurry.

Cerebral organoids

To generate cerebral organoids, PGP1 iPSCs were grown to ~80% confluence and, on day 0, were lifted from Matrigel-coated T225 flasks by incubation with gentle cell dissociation reagent for 12 min. The flasks were rinsed with DMEM/F12 containing Hepes and centrifuged for 5 min at 220g. Next, the cells were resuspended in EBCM and 10 μ M ROCKi and seeded into microwell arrays, prepared as described above, at a density of approximately 500 cells per microwell, and compacted by centrifugation at 100g for 3 min. The media was replaced on day 1 with fresh EBCM without ROCKi. On day 2, the EBs were measured to be approximately 200 μ m in diameter, and the media was replaced with neural induction medium (NIM) composed of DMEM/F12 with GlutaMAX, 1:1000 of heparin (10 mg/ml; Sigma-Aldrich), 1:100 N-2 supplement (Thermo Fisher Scientific), and 1 \times minimum essential medium nonessential amino acids (MEM-NEAA) (Thermo Fisher Scientific) with 1:2000 of 10 mM SB431542 in dimethyl sulfoxide (DMSO) (SB, EMD Millipore) and 1:2000 of 0.2 mM LDN 193189 in DMSO (LDN, EMD Millipore). Aliquots of SB and LDN were stored at -20°C and added to the other media components immediately before adding NIM to cells. On day 3, the OBBs were removed from the microwells by pipetting up and down with DMEM/F12 containing 15 mM Hepes buffer, and the aggregates were transferred to a 50-ml centrifuge tube. The OBBs were allowed to settle under gravity, the supernatant was aspirated, and then, the OBBs were resuspended in 6 ml of NIM per two microwell arrays that were harvested. Next, they were seeded into untreated T25 flasks, and 6 ml of NIM was mixed with the OBBs per flask. After harvesting, an additional 5 ml of NIM was pipetted into each flask. The flasks were transferred to an orbital shaker (VWR Shaker, 1000 Standard) that was set to 60 rpm and placed in an incubator. The media was replaced on days 5 and 7 by placing the flasks on a custom-built sedimentation rack that held the flask at 45° such that cells settle into a single corner of the T25 flask. Once settled, the supernatant was aspirated and replaced with 6 ml of fresh NIM. On day 8, the medium was replaced with neural differentiation medium (NDM) composed of a 1:1 mix of DMEM/F12 with Neurobasal medium (Thermo Fisher Scientific), 1:200 N-2 supplement (Thermo Fisher Scientific), 1:100 B27 without vitamin A (Thermo Fisher Scientific), 1:4000 insulin solution (Sigma-Aldrich), 1:100 GlutaMAX, and 1:200 MEM-NEAA. A 1000 \times solution of β -mercaptoethanol (1:1000; Thermo Fisher Scientific) was added to NDM immediately before adding the media to the OBBs. Thereafter, the media was replaced every other day, and the cerebral organoids were harvested for SWIFT vascularization on day 21.

Cardiac spheroids and EB-derived aggregates

To create the cardiac spheroids used for Fig. 1, D and E and fig. S2, we adapted a previous protocol by Lian *et al.* (28). Briefly, PGP1

iPSCs were grown to 80 to 95% confluence on T225 plates in mTeSR1 medium. Cardiac differentiation media was prepared by combining 500 ml of RPMI 1640 (Thermo Fisher Scientific) with either 10 ml of B27 without insulin (to form cardiomyocyte differentiation medium, CDM) or 10 ml of B27 (to form cardiomyocyte maturation medium, CMM). On day 0, differentiation was initiated by switching the mTeSR1 media to CDM and 6 μ M CHIR99021 for 24 hours. The following media changes were then made: day 1, CDM; day 3, CDM and 2 μ M iWR1 (BioGems; CDM); days 5 and 7, CDM; day 9 (or by day of beating), CMM; days 11 and 13, RPMI without glucose supplemented with 2% B27 (to purify cardiomyocytes); and day 15, CMM. In a separate T225 flask, primary ventricular normal human cardiac fibroblasts (Lonza) were cultured in stromal cell growth medium (Lonza). Next, cardiomyocytes, at day 17, and fibroblasts were passaged by rinsing with PBS and then incubated with TrypLE for 9 min (for cardiomyocytes) or 5 min (for fibroblasts) at 37°C. Next, the TrypLE was rinsed using 37°C DMEM, and the cells were pelleted into separate 15-ml tubes via centrifugation at 220g for 5 min. Both cell types were resuspended in cardiac spheroid medium (CSM), comprising DMEM with high glucose (American Type Culture Collection) containing 10% fetal bovine serum (FBS) and penicillin-streptomycin (100 U/ml). The cells were counted and combined at 70% cardiomyocytes and 30% fibroblasts and then seeded into molded 800- μ m-diameter PDMS microwells at a cell density of 2000 cells per microwell. The microwell arrays were centrifuged at 100g for 3 min to form OBBs from the cells. CSM was half-changed daily, and the cardiac spheroids were observed to be beating by 2 to 4 days after aggregation, at which point they were harvested for SWIFT vascularization.

To demonstrate the versatility of this process, we also generated cardiac OBBs according to a protocol adapted from (27) and (28). BJFF iPSCs were formed into EBs on day -4, as described above. Two T225s (at ~80% confluence) were used to seed four six-well plates of microwells. On day -3, to remove ROCKi, the media was replaced with 4 ml of EBCM. On day -2, EBs from two wells were harvested, combined, and allowed to settle under gravity. The supernatant was aspirated, and the EBs from two wells were resuspended in 12 ml of EBCM and transferred to a single untreated T25 flask. Thus, EBs from four six-well plates (i.e., 24 wells in total) were harvested and placed into 12 T25 flasks. These flasks were incubated on an orbital shaker with a rotational speed of 60 rpm. To maintain and differentiate the cells in the T25 flasks, the following media changes were performed: day -1, 12 ml of EBCM; days 0 and 1, 10 ml of CDM and 5 μ M CHIR99021 (BioGems) (CDMC); day 2, 10 ml of CDM; days 3 and 4, 10 ml of CDM; and day >5, 10 ml of CDM daily. On days 0, 2, and 5, a rinse was performed after aspiration, using 4 ml of the medium that the cells were being changed into, to increase the removal of growth factors or small molecules from the previous medium. After the cells resettled, the rinsing medium was removed before the new culture medium was added. Beating was typically initially observed by day 7, and almost all cardiac OBBs were visibly beating by day 9. SWIFT printing was performed using cardiac OBBs between days 9 and 11, after which the cells were maintained in CMM.

ECM preparation

An ECM prepolymer gel was prepared as follows: A transglutaminase (TG) working solution was first prepared by adding a microbial tissue TG formulation (20 mg/ml; Moo Gloo TI) to cell culture medium

(mTeSR1 for EBs, NIM for cerebral organoids) and sterile-filtering the solution via a 0.2-μm syringe filter. For cardiac OBBs, TG was not added to the ECM. Next, the volume (x milliliters) of high-concentration rat tail collagen I (Corning) required to create a collagen concentration (4 mg/ml) in the final ECM solution (total volume, y milliliters) was calculated. The ECM prepolymer gel solution composed of $(0.825y - 1.135x)$ ml of mTeSR1, 0.125 y ml of TG working solution (if applicable), $x/10$ ml of 10× PBS, $y/100$ ml of 250 mM CaCl₂, $\sim x/40$ ml of 1 N NaOH, x milliliters of high-concentration rat tail collagen type I, and 0.04 y ml of Matrigel was added, in order, on ice. For example, to generate 8 ml of ECM prepolymer gel using a solution of collagen I (8.90 mg/ml), the following was added in order: 2.56 ml of mTeSR1, 1 ml of mTeSR1 containing TG (20 mg/ml), 0.36 ml of 10× PBS, 0.080 ml of CaCl₂, 0.090 ml of 1 N NaOH, 3.596 ml of collagen I, and 0.320 ml of Matrigel. The volume of NaOH was adjusted, as necessary, to attain a final pH of ~ 7.4 . To prevent premature gelation, the pipette was precooled using ice-cold PBS before pipetting the collagen and Matrigel. After addition and mixing of all components, the gel was centrifuged at 2000g for 3 min at 2°C to remove air bubbles. The ECM prepolymer gel was stored on ice and used within ~ 1 hour.

Sacrificial ink preparation

A gelatin stock solution was used to prepare the sacrificial ink for SWIFT. The 15% (w/w) gelatin stock solution was made by slowly adding 45 g of gelatin into 255 ml of PBS without calcium or magnesium at 85°C while stirring. A separate gelatin ink was created for printing tissue molds used in the perfusion chambers following the same protocol temperature, except that a temperature of 70°C was used. In each case, the samples were held at temperature and stirred for 12 hours to fully dissolve the gelatin, after which their pH was adjusted, while stirring, to ~ 7.5 using 2 N NaOH. Each hot gelatin stock solution was sterile-filtered, aliquotted, and stored at 4°C for up to 6 months.

Cell density measurements

The EBs were harvested from the microwell arrays once they grew 200 to 250 μm in diameter (typically 2 to 4 days in microwell culture) by vigorous pipetting up and down in the wells with a P1000 pipette tip. The EB-containing media was transferred into a 50-ml tube, one tube per six wells. The wells were further rinsed with an excess of DMEM/F12 and Hepes using a 10-ml serological pipette to remove most (>90%) of the EBs. The media, with suspended EBs, was added to 50-ml centrifuge tubes, and the EBs were allowed to settle by incubating on ice for 10 min. All further cell handling was performed on ice to prevent gelation of the ECM. The supernatant was aspirated, and the EBs were collected into a single 50-ml tube. Next, 50 ml of fresh DMEM/F12 and Hepes was added to further wash away single cells. The EBs were then allowed to settle for another 10 min, and then, the supernatant was aspirated, and the EBs were resuspended up to 15 ml using DMEM/F12 and Hepes and transferred into a 15-ml tube and allowed to settle for 10 min. Next, to compact the EBs, the 15-ml tube was centrifuged at 100g for 3 min at 2°C, the supernatant was aspirated, and the total volume of the EB matrix was estimated. To replace the DMEM/F12 and Hepes in the extracellular space with ECM, the cells were rinsed in the ECM solution at a 1:3 (EB matrix:ECM solution) volume ratio by pipetting with a P1000 pipette and then centrifuged at 100g, and the supernatant was aspirated. Last, the consolidated EB-ECM solution was resuspended in an equal volume of

ECM solution, forming a dense EB-ECM slurry that could be handled and pipetted in subsequent steps. To estimate the cell density of the OBB matrix, the EB-ECM slurry was centrifuged at 150g for 3 min in an Eppendorf tube, and the OBB matrix volume was estimated visually by pipetting known volumes of water into a second Eppendorf tube to match the height of the pellet in the first tube. Next, the EBs were dissociated into single cells by incubating in Gentle Cell Dissociation Reagent for 15 min and triturating with a P1000 pipette, and the total cell number was counted. The cell density of the OBB matrix was then estimated by the ratio of cell number to OBB matrix volume.

Rheological measurements

Rheological measurements were carried out by first compacting the prepared EB, ECM, and EB-ECM slurries (mean diameter of EBs, ~ 200 μm) into 3-cm³ syringes (Nordson EFD) and then extruding them directly onto the rheometer plate of a TA-instruments Discovery HR-3 stress-controlled rheometer. The plate, with a diameter of 25 mm, was precooled to 2°C. Both the plate and disc were coated with sandpaper to prevent wall slip, and the gap height was brought to 1 mm. Any excess slurry was trimmed with a spatula before these measurements. First, oscillatory frequency sweeps were performed from 0.1 to 10 rad/s with an applied shear stress of 0.5 Pa. Next, oscillatory amplitude sweeps were performed from 0.01 to 100 Pa at a frequency of 0.5 Hz. Apparent viscosities were determined by flow sweeps performed from shear rates of 0.01 to 5/s. The EB matrix yield stress was estimated by fitting a Herschel-Bulkley curve to the increasing shear-rate sweep. Next, to measure the gelation of the ECM upon raising the temperature, the storage and loss moduli were probed with an oscillatory shear stress of 5 Pa and a frequency of 0.5 Hz at 2°C before raising the temperature to 37°C and lowering the gap height to 900 μm to account for EB matrix shrinkage after gelation. To measure gelatin ink rheology, the sacrificial ink was prepared in a 0.5-cm³ glass syringe (Hamilton) and extruded through a 1.5-inch straight metal nozzle with an inner diameter of 250 μm (Nordson EFD). The printed gelatin was collected and transferred onto the rheometer, which was set up as described above.

Silicone mold and perfusion chamber fabrication

Direct ink writing was used to manufacture customized silicone molds for printing and perfusing bulk tissues. First, a printable silicone ink was prepared by combining a 10:1 mass ratio of SE1700 base:curing agent (Dow Corning) and then adding 1% (w/w) black silicone pigment (Silc-Pig, Smooth-On). The components were then mixed using a speed mixer for 3 min at 2000 rpm (THINKY Inc.). Using a spatula, freshly mixed silicone ink was loaded into a 30-cm³ syringe (Nordson EFD) and centrifuged at >3000g to remove entrapped air. A tapered nozzle with a 0.41-mm inner diameter tip (Nordson EFD) was attached to the outlet of the syringe, and the syringe was affixed to a custom 3D printer (26). Ink was dispensed from the syringe by means of pressure generated by an Ultimus V pressure controller (Nordson EFD) onto an underlying glass substrate. The tissue molds are composed of silicone walls and small channels for tube-insertion sites, i.e., inlets and outlets. After printing, each mold was transferred to 80°C for >2 hours to cure. After curing, fresh silicone ink was extruded onto the top layer of the mold (either manually or using the 3D printer), and a second glass slide was added to the top, such that the silicone gasket was sandwiched between two glass slides. For the mold used in Fig. 3, clear silicone was printed and cured onto the second glass

slide before assembly, such that the assembled gasket had a slit in the middle of the top side for nozzle insertion. The mold was transferred to 80°C to cure the silicone. Stainless steel tubes serving as inlets and outlets with an inner diameter of 0.83 mm were inserted into the inlet/outlet channels of the molds used for perfusion, and Versilon silicone tubing, with an inner diameter of $1/32$ inches, was fitted to the external ends of the tubes and crimped with a hose clamp to seal the inlets and outlets. For the custom perfusion mold in Fig. 3, the stainless-steel tubes had a small ~1-mm notch cut into one end to facilitate a continuous connection from the printed vascular channels and the tube. Molds were autoclaved and stored at room temperature before use.

Alternately, polycarbonate chambers and front and back plates were machined to produce custom perfusion devices (fig. S7). The use of glass windows allowed for tissue visualization, and watertight seals were formed between the windows and chamber walls via o-rings. Metal tubes serving as fluidic inlets and outlets were press-fit on the side and bottom of the chamber. The perfusion chambers were autoclaved and stored at room temperature before use. Before printing vascular channels inside the OBB-based matrices, an anchoring structure was printed using a stereolithography 3D printer (Perfactory Aureus, Envisiontec, Inc), using E-Shell 300 clear resin, postcured under ultraviolet (UV) illumination, and positioned within the chamber. This structure had a pair of anchoring prongs for embedding inside the tissue, which served to hold the tissue in place during perfusion, while allowing for media perfusion around the outer surfaces of the tissue. Next, a tissue template (which ultimately forms the shape of the tissue) was stereolithographically printed, postcured under UV illumination, plasma-treated, and dipped into a 10% (w/w) aqueous solution of Pluronic F-127 (Sigma) and allowed to air-dry. This Pluronic F127-coated template was inserted into the chamber and was fitted over the anchoring prongs. Next, 5% (w/v) molten gelatin, prepared by adding PBS to a stock solution of 15% (w/v) gelatin, was poured into the chamber and injected into the side metal tubes and allowed to gel around the template at 4°C for 15 min. The template was then removed by pulling straight up, leaving a tissue mold with a custom tissue geometry and anchoring prongs protruding at its top. An o-ring was placed around the tissue inlet tube located at the bottom of the mold after which the printer was aligned to the chamber. To form a tissue-anchoring plug around the inlet, a solution of high-concentration ECM (hcECM) was prepared similar to the ECM described above, but with collagen (7.5 mg/ml) and 2% (w/v) TG [from a stock of TG (160 mg/ml) in medium]. This material was dispensed at the base of the tissue mold and around the O-ring before gelling at 22°C for 15 min. Last, 5% (w/v) molten gelatin was injected into the bottom metal pin before filling the mold with an uncompacted mix of cell aggregate and ECM solution for SWIFT printing.

Cardiac mold design and fabrication

A 3D computer-aided design (CAD) model of a normal 17-year-old heart was downloaded from the NIH 3D Print Exchange in the form of a stereolithography (.stl) file. The model was first rotated to orient the apex downward, and a section of the myocardium was digitally truncated using Tinkercad (Autodesk). The geometry was then alternatively smoothed and simplified in MeshLab to eliminate the noise and asperities of the model surface. Tinkercad was next used to generate positive and negative models of the desired geometry and to digitally carve out a wedge in the section of the anterior

wall and the septum, in the vicinity of the LAD coronary artery, which subsequently served as a reservoir for the cardiac OBB matrix. These models were built at a 1:2 scale using an Objet30 3D printer (Stratasys) to serve as masters for the casting of the final heart visualization model and cardiac tissue receptacle. This three-step process consisted of the casting of a transparent block of PDMS (SYLGARD 184 at 10:1 base:curing agent) off of the outer surface of the sectioned myocardium master, the casting of the actual truncated myocardium using a lightly colored PDMS (using red and white Silc-Pig in SYLGARD 184), and the assembly of those two parts with PDMS acting as glue and filling the ventricles. A 3D printed wedge plug was used during the curing step to ensure that the cardiac tissue wedge reservoir remained open. The print path was generated by extracting the LAD and one of its diagonal branches from the original CAD model. The stereolithography file was sliced, and a MATLAB routine was used to skeletonize the vascular channels and convert it into GCode. Because of the low resolution of the CAD model, only a portion of the LAD and a single diagonal could be extracted from patient data; extra septal and diagonal branches were manually added to the coronary vasculature print path, using geometries similar to those found *in vivo*.

Sacrificial writing into functional tissues

A sacrificial gelatin ink was prepared using the procedure described above to enable embedded 3D printing of vascular networks. The gelatin stock solution (solubilized at 85°C, as described above) was melted at 80°C for <30 min and then diluted in PBS to generate a 5% (w/v) solution. Next, red food coloring was added at 2% (v/v) to enable visualization of printed ink. The freshly prepared sacrificial gelatin ink was loaded into a 0.5-cm³ glass syringe and subsequently cooled to 4°C for 15 min to induce gelation. The glass syringe was then loaded onto a custom-built syringe pump that was mounted onto the 3D printer. The syringe pump was operated by an Arduino microcontroller and a stepper-motor driver. The syringe barrel was housed in a water-cooled custom-built temperature controller to control the stiffness of the gelatin ink by maintaining a temperature of approximately 20°C. A metal nozzle, with a length of 1.5 inches and an inner diameter of 0.25 mm (Nordson EFD), was fitted to the bottom of the syringe. Before printing, the syringe was incubated in its temperature-controlled housing for >15 min.

The OBB-ECM matrix was loaded into the silicone molds or perfusion chambers, and the following steps were performed rapidly to ensure that it remained cold and that the ECM did not undergo gelation before SWIFT was completed. First, for cardiac tissue fabrication, the volume of cardiac OBBs was estimated by compacting via centrifugation at 100g. Next, the ECM solution was mixed with 10^7 HNDF cells/ml of cardiac OBBs before resuspending the cardiac OBBs in the ECM:HNDF cell mixture to generate a slurry. The freshly prepared OBB slurry was pipetted into the molds, and the molds and their housing were centrifuged at 150g at 2°C for 3 min to compact the aggregates, forming an OBB-based matrix, containing $\sim 2.4 \times 10^8 \pm 0.4 \times 10^8$ cells/ml and $6 \times 10^5 \pm 2 \times 10^5$ HNDF cells/ml. Most of the supernatant ECM was removed leaving ~1 mm of the ECM solution above the top of the compacted bed of OBBs. To keep the matrix cool during the long-duration print in Fig. 3 (C and D), the mold was transferred onto the front of a custom-built water-cooled metal plate, comprising a metal plate, backed by an acrylic sheet that had milled channels through which ice-cold water was pumped. Both the metal plate and the acrylic sheet were cut to enable back

illumination to facilitate visualization of the printing process. The mold was held on the water-cooled plate by a pair of clamps and was maintained in its housing in a vertical orientation by pressing it against two metal right-triangle prisms.

The desired vascular network was then printed within the OBB-based matrix at a print speed ranging from 0.5 to 4 mm/s. The extrusion rate of the syringe pump was set to define a certain diameter filament. The vascular geometry was designed in a custom-built MATLAB script that generated branched cubic splines, automatically assigned a printing order to prevent the nozzle from translating through previously printed features, and rendered each curvilinear line as piecewise linear segments in GCode. To vary the filament (and, hence, channel) diameter, the print speed was changed while maintaining a constant ink deposition. After each line segment, ink extrusion is stopped, and to avoid agitating the printed patterns, the nozzle was withdrawn vertically above the top of the tissue, translated to its new x and y coordinates, and reinserted to the correct new z coordinate by moving down vertically.

Design of hierarchical vascular networks

When templating a complex hierarchical vascular network (Fig. 3, C and D), the channel diameters were computed to ensure an equivalent shear stress within each segment of the network, independent of their diameter. Assuming Poiseuille flow, we determined the channel radius R and the flow Q , along with the pressure P at each node by solving the following set of equations (in MATLAB). On the basis of mass conservation, the sum of flow coming to a node is zero

$$\sum_i Q_i = 0$$

The flow Q through each segment is proportional to the fourth power of its radius R^4 and the difference of pressure across ΔP , as given by

$$Q = \frac{\pi R^4}{8\eta l} \Delta P$$

where η is the viscosity of the culture medium and l is the length of a given segment. The shear stress exerted on a vessel wall, $\tau = \frac{4\eta Q}{\pi R^3}$, should be constant throughout the network, hence

$$\frac{Q_i}{R_i^3} = \frac{Q_1}{R_1^3}$$

For the vascular network depicted in Fig. 3 (C and D), the ratio between the largest vessels (inlet and outlet) and the smallest one was found to be 1.3. To print these channels at a constant deposition rate, the nozzle velocity was modulated proportionally to the inverse of the square of the diameter of each channel (or to its cross-sectional area).

Perfusion of SWIFT tissue constructs

After SWIFT printing of cardiac tissues in machined perfusion chambers, the tissue was capped with hcECM to provide mechanical stability required to maintain patency for long-term culture. The mold was then transferred to a 37°C, 5% CO₂ incubator for 45 min to complete gelation of the OBB-ECM matrix, and to melt the printed sacrificial gelatin filaments and gelatin that surrounds the tissue. After incubation, silicone molds were sealed via an excess of autoclaved SE1700 silicone base (without cross-linker) into the gap at

the top of the mold, while machined perfusion chambers were sealed by screwing on the polycarbonate lid. The sealed perfusion devices were then transferred to a custom-made tissue perfusion housing that held the tissue vertically and adjacent to a media reservoir, containing mTeSR1 media with PVA (4 mg/ml; for EB perfusion) or CMM (for cardiac tissue perfusion) with 1% antibiotic-antimycotic (Thermo Fisher Scientific). Next, the tissue was maintained at 37°C, where the sacrificial gelatin ink is molten, and a peristaltic pump (Ismatec Inc.) was used to introduce fluid media that removes the gelatin and leaves behind open channels. For the cardiac tissue perfusion, after evacuating the printed gelatin at a vascular flow rate of 0.01 ml/min for 5 min, the inlet for the external perfusion was opened, and the molten gelatin that surrounds the cardiac tissue was evacuated at a high perfusion rate (0.8 ml/min) for 5 min. To ensure the removal of all gelatin, this process was repeated but with a vascular perfusion rate of 0.02 ml/min. Over the course of ~1 hour, the perfusion rate was then increased gradually to its final perfusion rate. Perfusion rates used are 250 µl/min for Fig. 3 (C and D), 100 µl/min for EB-tissue perfusion for viability measurements, and 500 µl/min for cardiac tissue perfusion. For specific experiments, the media reservoir was hyperoxygenated by means of bubbling a mixture of sterile-filtered 95% O₂/5% CO₂ (Airgas Inc.) through the media at a volumetric flow rate of ~10 ml/min.

Cell viability assays

For EB viability measurements, the tissues were removed from flow after 12 hours of perfusion. Next, the tissues and their molds were first immersed in a large bath of ice-cold PBS. The perfusion chambers were opened by unscrewing the front panel and removing the glass window. The tissues were then sectioned using a pair of microdissection scissors and transferred via aspiration into a 35-mm petri dish containing a cut silicone gasket to house the tissue for imaging. Next, the PBS was changed to mTeSR1 and PVA medium (4 mg/ml) by repeatedly flushing ~50% of the volume at a time with fresh mTeSR1. An equal volume of 2× concentrate LIVE/DEAD solution [calcein (1 µl/ml), ethidium homodimer-1 (EthD-1, 4 µl/ml), and Hoechst solution (0.5 µl/ml)] was then added, and the tissue was incubated at 37°C for 30 min. After incubation, LIVE/DEAD images were acquired on a confocal microscope (ZEISS) using a 5× ApoFluor objective. A cell number-normalized viability score was calculated as the ratio of the area of a thresholded calcein-AM viability signal to the area of a thresholded Hoechst signal. To obtain cell viability data for cardiac tissues, the same process was used. However, the tissues were incubated on ice immediately before imaging to suppress beating artifacts during imaging.

Lumen endothelialization

Before endothelialization, an EB-based tissue featuring a SWIFT-printed single vessel was perfused with DMEM:F12 supplemented with 1% (v/v) of Matrigel for 20 min to enhance endothelial cell adhesion. HUVECs, cultured in EGM2 medium, were harvested from their flasks by incubating for 5 min in 0.05% trypsin/EDTA. The cells were centrifuged at 220g in DMEM with 10% FBS, strained, and resuspended at a density of 10⁷ cells/ml in EGM2. The HUVEC suspension was perfused through the lumen at a flow rate of 40 µl/min until they could be seen exiting the tissue. The flow was then stopped, and the tissue gasket was laid flat for 10 min in the incubator to allow cells to settle at the surface of the lumen. This process was repeated three times, each time laying the gasket flat at a different

angle such that the four quadrants of the lumen were coating with HUVECs. Tissues were then returned to being perfused with 1:1 mTSer1:EGM2 medium at a flow rate of 40 μ l/min for 24 hours before being fixed for analysis.

Calcium imaging

A concentrated solution of Rhod-2 (Thermo Fisher Scientific) was prepared by dissolving 50 μ g of the calcium indicator in 100 μ l of DMSO. The solution was then diluted 1:250 in Tyrode's solution (Alfa Aesar). Blebbistatin (Sigma-Aldrich) was added at a final concentration of 5 μ M (from a 5 mM stock solution). Cardiac OBB tissues were first rinsed with Tyrode's solution (Alfa Aesar) and incubated with the calcium indicator solution for 30 min. Next, the tissues were rinsed once with a blebbistatin-containing Tyrode's solution. The samples were subjected to a 555-nm light illumination, and the wide-field signal was captured by a scientific complementary metal-oxide semiconductor camera (sCMOS, Andor technology). Data were acquired using Micro-Manager open source software. During imaging, the plate containing the cardiac tissues was placed on top of a heated pad (Stoelting).

Electrical stimulation

To electrically stimulate the SWIFT cardiac tissues within the perfusion chamber, the back panel was replaced with a plate featuring two platinum wires (0.25 mm in diameter) looped into rectangles (14 mm by 5 mm) and such that both platinum wires were located 15 mm apart when mounted onto the perfusion chamber. A monophasic signal with a pulse of 2 ms was generated by a custom-made Arduino-based controller at a frequency of 1 or 2 Hz and an amplitude of 6 V/cm. For point stimulation of cardiac OBB tissue in fig. S12 and movie S6, the electrodes were composed of the same platinum wires but with extremities placed at a distance of 750 μ m from one another and were positioned near the tissue to stimulate with a manual micromanipulator. The voltage was set to 20 V to trigger pacing of the tissue.

Pharmacological assays

On day 8, calcium was supplemented to the culture medium to a final concentration of 2 mM. Cardiac tissues were perfused for 20 min before videos were acquired. Then, isoproterenol (Sigma-Aldrich) was administered intraluminally for 20 min to cardiac tissues at a concentration of 10 μ M before they were imaged again. On separate sets of experiments, 1-heptanol (Sigma-Aldrich) was added to the medium on day 11 at a concentration of 1 mM, and cardiac tissues were perfused intraluminally for 20 min, after which each tissue was imaged. Beating patterns were acquired by tracking the anchoring prongs of the cardiac tissue using the software Tracker (physlets.org/tracker).

Cryosectioning, immunostaining, and flow cytometry

Tissues were cryosectioned by first fixing for 30 min in 4% formaldehyde and then rinsed three times in PBS containing 0.05% Tween 20 detergent (PBST). The fixed tissue was incubated overnight at 4°C in PBS containing 30% sucrose (sucrose solution) and then transferred into a 1:1 solution of Optimal Cutting Temperature compound:sucrose (OCT:sucrose) for 1 hour and 30 min. Next, the tissue was gently placed into a cryostat tissue mold, which was subsequently filled with 100% OCT solution and frozen on a cryostat Peltier cooler. The tissue was sectioned using 40- to 60- μ m slices

and transferred onto a Superfrost Plus slide (VWR Inc.). Sections were stored at -20°C before immunostaining.

For immunostaining, the tissue cryosections were first permeabilized in a 0.125% solution of Triton X containing 0.5% bovine serum albumin (BSA) or 2% donkey serum (DS) for 10 min, rinsed three times in PBST, and blocked for at least 30 min in a solution of PBS containing 3% BSA or 2% DS. Next, primary antibodies [Oct 4 (1:200; sc-5279, Santa Cruz Biotechnology), Sox 2 (1:40; AF2018, R&D Systems), Tuj1 (1:1000; MAB1195, R&D Systems), collagen I (1:500; ab90395, Abcam), cTnT (1:200; ab45932, Abcam), and sarcomeric α -actinin (1:200; ab9465, Abcam)] were added in 3% BSA or 2% DS in PBS and incubated overnight at 4°C. On the following day, the primary antibody was removed by rinsing three times in PBST, and Alexa Fluor Plus-conjugated secondary antibodies were added at 1:400 in 3% BSA or 2% DS in PBS for 45 min. The secondary antibodies were removed by rinsing three times in PBST. The nuclei were then labeled using a 1:5000 dilution of 4',6-diamidino-2-phenylindole in PBS for 3 min, followed by rinsing twice with PBST. The sections were imaged using a Zeiss confocal microscope.

To carry out flow cytometry, after measuring its volume (as described above for EB density estimation), the cardiac OBB matrix was rinsed thoroughly with cold DMEM to remove ECM. The remaining cardiac OBBs were dissociated by incubation for 30 min at 37°C in a papain solution [papain (25 U/ml) in Earl's balanced salt solution containing L-cysteine and EDTA, per the manufacturer's instructions (Worthington, Inc.)]. The cells were rinsed in fresh CDM, triturated via repeated pipetting with a P1000 pipette tip, and counted using a hemocytometer. The cells were then rinsed twice in PBS containing 3% BSA, fixed by incubating with CytoFix (BD Biosciences) for 15 min at 4°C and then rinsed twice via centrifugation and addition of PBS containing 3% BSA. For flow cytometry, 1×10^6 cells were resuspended in perm-wash solution (BD Biosciences) and incubated for 15 min at room temperature before rinsing in fresh perm-wash solution. Next, samples were blocked for 15 min at room temperature by incubation in Pharmingen solution (BD Bioscience). The cells were then incubated for 1 hour in labeled primary antibodies (Vimentin PE, 562337, BD Pharmingen; cTnT Alexa Fluor 647, 565744, BD Pharmingen; 1:10 dilution in Pharmingen solution). After incubation, cells were washed twice in perm-wash and analyzed using an LSR II Analyzer (BD Biosciences). Gating of cell populations was performed as shown in fig. S10.

SUPPLEMENTARY MATERIALS

Supplementary material for this article is available at <http://advances.sciencemag.org/cgi/content/full/5/9/eaaw2459/DC1>

Supplementary Materials and Methods

Fig. S1. OBB displacement during SWIFT.

Fig. S2. Luminal channels formed after sacrificial ink printing and removal.

Fig. S3. Rheological characterization of tissue matrix constituents.

Fig. S4. Tissue viability assessment.

Fig. S5. Branching vascular network embedded within an EB-based tissue matrix via SWIFT.

Fig. S6. Embedded 3D printing of OBBs within different living matrices.

Fig. S7. Schematic illustrations of perfusion apparatus for SWIFT biomanufacturing and tissue maintenance.

Fig. S8. Viability of perfused and nonperfused EB-based tissues.

Fig. S9. Custom-made perfusion chip for large-scale viability assay.

Fig. S10. Flow cytometry data for cardiac OBBs.

Fig. S11. Cardiac tissue composition.

Fig. S12. Calcium imaging of cardiac tissue matrix.

Fig. S13. Characterization of cardiac tissue produced by SWIFT.

Fig. S14. Characterization of perfused cardiac tissue.

Movie S1. Nozzle translation during embedded printing within a tissue matrix composed of OBBs.

Movie S2. Biomanufacturing of a helical vascular feature within a tissue matrix composed of OBBs.

Movie S3. Biomanufacturing of a branched vascular network within a tissue matrix composed of OBBs.

Movie S4. Endothelialization of a vascular channel within a tissue matrix composed of OBBs.

Movie S5. OBBs composed of beating cardiac organoids.

Movie S6. Calcium imaging of cardiac OBB matrix.

Movie S7. Cardiac tissues with perfusable vascular channels via SWIFT.

Movie S8. Contractile activity of a bulk cardiac tissue (T-shaped construct) produced by SWIFT biomanufacturing.

REFERENCES AND NOTES

1. J. S. Miller, The billion cell construct: Will three-dimensional printing get us there? *PLOS Biol.* **12**, e1001882 (2014).
2. T. Takebe, K. Sekine, M. Enomura, H. Koike, M. Kimura, T. Ogaeri, R.-R. Zhang, Y. Ueno, Y.-W. Zheng, N. Koike, S. Aoyama, Y. Adachi, H. Taniguchi, Vascularized and functional human liver from an iPSC-derived organ bud transplant. *Nature* **499**, 481–484 (2013).
3. W.-H. Zimmermann, I. Melnychenko, G. Wasmeier, M. Didié, H. Naito, U. Nixdorff, A. Hess, L. Budinsky, K. Brune, B. Michaelis, S. Dhein, A. Schwoerer, H. Ehmke, T. Eschenhagen, Engineered heart tissue grafts improve systolic and diastolic function in infarcted rat hearts. *Nat. Med.* **12**, 452–458 (2006).
4. M. Radisic, H. Park, H. Shing, T. Consi, F. J. Schoen, R. Langer, L. E. Freed, G. Vunjak-Novakovic, Functional assembly of engineered myocardium by electrical stimulation of cardiac myocytes cultured on scaffolds. *Proc. Natl. Acad. Sci. U.S.A.* **101**, 18129–18134 (2004).
5. R. L. Carrier, M. Papadaki, M. Rupnick, F. J. Schoen, N. Bursac, R. Langer, L. E. Freed, G. Vunjak-Novakovic, Cardiac tissue engineering: Cell seeding, cultivation parameters, and tissue construct characterization. *Biotechnol. Bioeng.* **64**, 580–589 (1999).
6. I. Y. Shadrin, B. W. Allen, Y. Qian, C. P. Jackman, A. L. Carlson, M. E. Juhas, N. Bursac, Cardiopatch platform enables maturation and scale-up of human pluripotent stem cell-derived engineered heart tissues. *Nat. Commun.* **8**, 1825 (2017).
7. G. C. Engelmayr Jr., M. Cheng, C. J. Bettinger, J. T. Borenstein, R. Langer, L. E. Freed, Accordion-like honeycombs for tissue engineering of cardiac anisotropy. *Nat. Mater.* **7**, 1003–1010 (2008).
8. M. Juhas, G. C. Engelmayr Jr., A. N. Fontanella, G. M. Palmer, N. Bursac, Biomimetic engineered muscle with capacity for vascular integration and functional maturation in vivo. *Proc. Natl. Acad. Sci. U.S.A.* **111**, 5508–5513 (2014).
9. K. R. Stevens, M. A. Scull, V. Ramanan, C. L. Fortin, R. R. Chaturvedi, K. A. Knoose, J. W. Xiao, C. Fung, T. Mirabella, A. X. Chen, M. G. McCue, M. T. Yang, H. E. Fleming, K. Chung, Y. P. de Jong, C. S. Chen, C. M. Rice, S. N. Bhatia, In situ expansion of engineered human liver tissue in a mouse model of chronic liver disease. *Sci. Transl. Med.* **9**, eaah5505 (2017).
10. N. F. Huang, V. Serpooshan, V. B. Morris, N. Sayed, G. Pardon, O. J. Abilez, K. H. Nakayama, B. L. Pruitt, S. M. Wu, Y.-s. Yoon, J. Zhang, J. C. Wu, Big bottlenecks in cardiovascular tissue engineering. *Commun. Biol.* **1**, 199 (2018).
11. D. B. Kolesky, K. A. Homan, M. A. Skylar-Scott, J. A. Lewis, Three-dimensional bioprinting of thick vascularized tissues. *Proc. Natl. Acad. Sci. U.S.A.* **113**, 3179–3184 (2016).
12. J. S. Miller, K. R. Stevens, M. T. Yang, B. M. Baker, D.-H. T. Nguyen, D. M. Cohen, E. Toro, A. A. Chen, P. A. Galie, X. Yu, R. Chaturvedi, S. N. Bhatia, C. S. Chen, Rapid casting of patterned vascular networks for perfusable engineered three-dimensional tissues. *Nat. Mater.* **11**, 768–774 (2012).
13. B. Grigoryan, S. J. Paulsen, D. C. Corbett, D. W. Sazer, C. L. Fortin, A. J. Zaita, P. T. Greenfield, N. J. Calafat, J. P. Gounley, A. H. Ta, F. Johansson, A. Randles, J. E. Rosenkrantz, J. D. Louis-Rosenberg, P. A. Galie, K. R. Stevens, J. S. Miller, Multivascular networks and functional intravascular topologies within biocompatible hydrogels. *Science* **364**, 458–464 (2019).
14. L. E. Niklason, R. S. Langer, Advances in tissue engineering of blood vessels and other tissues. *Transpl. Immunol.* **5**, 303–306 (1997).
15. X. Yin, B. E. Mead, H. Safaei, R. Langer, J. M. Karp, O. Levy, Engineering stem cell organoids. *Cell Stem Cell* **18**, 25–38 (2016).
16. M. A. Lancaster, M. Renner, C.-A. Martin, D. Wenzel, L. S. Bicknell, M. E. Hurles, T. Homfray, J. M. Penninger, A. P. Jackson, J. A. Knoblich, Cerebral organoids model human brain development and microcephaly. *Nature* **501**, 373–379 (2013).
17. M. Takasato, P. X. Er, H. S. Chiu, B. Maier, G. J. Baillie, C. Ferguson, R. G. Parton, E. J. Woltvetang, M. S. Roost, S. M. Chuva de Sousa Lopes, M. H. Little, Kidney organoids from human iPSCs contain multiple lineages and model human nephrogenesis. *Nature* **526**, 564–568 (2015).
18. R. Morizane, A. Q. Lam, B. S. Freedman, S. Kishi, M. T. Valerius, J. V. Bonventre, Nephron organoids derived from human pluripotent stem cells model kidney development and injury. *Nat. Biotechnol.* **33**, 1193–1200 (2015).
19. K. A. Homan, N. Gupta, K. T. Kroll, D. B. Kolesky, M. Skylar-Scott, T. Miyoshi, D. Mau, M. T. Valerius, T. Ferrante, J. V. Bonventre, J. A. Lewis, R. Morizane, Flow-enhanced vascularization and maturation of kidney organoids in vitro. *Nat. Methods* **16**, 255–262 (2019).
20. K. Breckwoldt, D. Lettuce-Breniere, I. Mannhardt, T. Schulze, B. Ulmer, T. Werner, A. Benzin, B. Klampe, M. C. Reinsch, S. Laufer, A. Shibamiya, M. Prondzynski, G. Mearini, D. Schade, S. Fuchs, C. Neuber, E. Krämer, U. Saleem, M. L. Schulze, M. L. Rodriguez, T. Eschenhagen, A. Hansen, Differentiation of cardiomyocytes and generation of human engineered heart tissue. *Nat. Protoc.* **12**, 1177–1197 (2017).
21. W. Wu, A. DeConinck, J. A. Lewis, Omnidirectional printing of 3D microvascular networks. *Adv. Mater.* **23**, H178–H183 (2011).
22. M. Wehner, R. L. Truby, D. J. Fitzgerald, B. Mosadegh, G. M. Whitesides, J. A. Lewis, R. J. Wood, An integrated design and fabrication strategy for entirely soft, autonomous robots. *Nature* **536**, 451–455 (2016).
23. T. Bhattacharjee, S. M. Zehnder, K. G. Rowe, S. Jain, R. M. Nixon, W. G. Sawyer, T. E. Angelini, Writing in the granular gel medium. *Sci. Adv.* **1**, e1500655 (2015).
24. T. J. Hinton, Q. Jalleral, R. N. Palchesko, J. H. Park, M. S. Grodzicki, H.-J. Shue, M. H. Ramandan, A. R. Hudson, A. W. Feinberg, Three-dimensional printing of complex biological structures by freeform reversible embedding of suspended hydrogels. *Sci. Adv.* **1**, e1500758 (2015).
25. C. B. Highley, C. B. Rodell, J. A. Burdick, Direct 3D printing of shear-thinning hydrogels into self-healing hydrogels. *Adv. Mater.* **27**, 5075–5079 (2015).
26. A. K. Grosskopf, R. L. Truby, H. Kim, A. Perazzo, J. A. Lewis, H. A. Stone, Viscoplastic matrix materials for embedded 3D printing. *ACS Appl. Mater. Interfaces* **10**, 23353–23361 (2018).
27. H. Kempf, C. Kropf, R. Olmer, U. Martin, R. Zweigerdt, Cardiac differentiation of human pluripotent stem cells in scalable suspension culture. *Nat. Protoc.* **10**, 1345–1361 (2015).
28. X. Lian, C. Hsiao, G. Wilson, K. Zhu, L. B. Hazeltine, S. M. Azarin, K. K. Raval, J. Zhang, T. J. Kamp, S. P. Palecek, Robust cardiomyocyte differentiation from human pluripotent stem cells via temporal modulation of canonical Wnt signaling. *Proc. Natl. Acad. Sci. U.S.A.* **109**, E1848–E1857 (2012).
29. C. Bussadori, A. Moreo, M. Di Donato, B. De Chiara, D. Negura, E. Dall'Aglie, E. Lobiati, M. Chessa, C. Arcidiacono, J. S. Dua, F. Mauri, M. Carminati, A new 2D-based method for myocardial velocity strain and strain rate quantification in a normal adult and paediatric population: Assessment of reference values. *Cardiovasc. Ultrasound* **7**, 8 (2009).
30. N. Noor, A. Shapira, R. Edri, I. Gal, L. Wertheim, T. Dvir, 3D printing of personalized thick and perfusable cardiac patches and hearts. *Adv. Sci.* **6**, 1900344 (2019).

Acknowledgments: We thank J. Weaver for 3D printing cardiac molds and perfusion hardware, D. Mau for assistance in cell culture, S. Cotreau and the Harvard SEAS Machine Shop for the manufacturing of printing platforms, D. Foresti for constructing the temperature control system used for gelatin cooling, Srikanth Damaraju for consultations on coronary artery morphology, T. Ferrante for his assistance with calcium imaging, and L. K. Sanders for photography of printed tissue constructs. **Funding:** This research was primarily funded by the Office of Naval Research Vannevar Bush Faculty Fellowship program under award number N000141612823. Additional support was provided by the NSF CELL-MET (award number EEC-1647837), the National Human Genome Research Institute of the NIH under award number R01HG008525 (cerebral organoids), GETTYLAB, and the 3D Organ Engineering Initiative at the Wyss Institute. **Author contributions:** M.A.-S., S.G.M.U., and J.A.L. designed research; M.A.-S., S.G.M.U., L.L.N., J.H.A., R.L.T., and S.D. performed research; M.A.-S. and S.G.M.U. analyzed data; and M.A.-S., S.G.M.U., and J.A.L. wrote the manuscript. **Competing interests:** J.A.L., M.A.-S., and S.G.M.U. are inventors on a patent application related to this work filed by Harvard University (no. PCT/US18/51901, filed on 20 September 2018). The authors declare that they have no other competing interests. **Data and materials availability:** All data needed to evaluate the conclusions in the paper are present in the paper and/or the Supplementary Materials. Additional data related to this paper may be requested from the authors.

Submitted 1 December 2018

Accepted 2 August 2019

Published 6 September 2019

10.1126/sciadv.aaw2459

Citation: M. A. Skylar-Scott, S. G. M. Uzel, L. L. Nam, J. H. Ahrens, R. L. Truby, S. Damaraju, J. A. Lewis, Biomanufacturing of organ-specific tissues with high cellular density and embedded vascular channels. *Sci. Adv.* **5**, eaaw2459 (2019).

Science Advances

Biomanufacturing of organ-specific tissues with high cellular density and embedded vascular channels

Mark A. Skylar-Scott, Sébastien G. M. Uzel, Lucy L. Nam, John H. Ahrens, Ryan L. Truby, Sarita Damaraju and Jennifer A. Lewis

Sci Adv **5** (9), eaaw2459.
DOI: 10.1126/sciadv.aaw2459

ARTICLE TOOLS

<http://advances.sciencemag.org/content/5/9/eaaw2459>

SUPPLEMENTARY MATERIALS

<http://advances.sciencemag.org/content/suppl/2019/08/29/5.9.eaaw2459.DC1>

REFERENCES

This article cites 30 articles, 8 of which you can access for free
<http://advances.sciencemag.org/content/5/9/eaaw2459#BIBL>

PERMISSIONS

<http://www.sciencemag.org/help/reprints-and-permissions>

Use of this article is subject to the [Terms of Service](#)

Science Advances (ISSN 2375-2548) is published by the American Association for the Advancement of Science, 1200 New York Avenue NW, Washington, DC 20005. The title *Science Advances* is a registered trademark of AAAS.

Copyright © 2019 The Authors, some rights reserved; exclusive licensee American Association for the Advancement of Science. No claim to original U.S. Government Works. Distributed under a Creative Commons Attribution NonCommercial License 4.0 (CC BY-NC).